Uncommon Solution Behavior of Poly(*N*-vinylimidazole). Angular Dependence of Scattered Light from Aggregates in Ethanol

Gabriela Savin[†,‡] and Walther Burchard*[,†]

Institute of Macromolecular Chemistry, Albert-Ludwig-University Freiburg, 70104 Freiburg, Germany, and "Transilvania" University of Brasov, 2200 Brasov, Romania

Received September 12, 2003; Revised Manuscript Received February 6, 2004

ABSTRACT: Static light scattering measurements from high molar mass poly(*N*-vinylimidazole) (PVI) in ethanol displayed strikingly different angular dependencies from the PVI samples below $M_w = 8 \times 10^5$ g/mol. The high molar mass particles were considered as aggregates. A classification of the aggregate structure became possible by comparison with different, well-understood models. The shapes of the curves were examined, on one hand, on the basis of one-component models, with heterogeneity in segment density, and on the other, on the assumption of a two-component system. The observed scattering curves show behavior similar to the soft-sphere model and in another aspect to star-branched macromolecules with stiff arms. Also, a two-component analysis of the scattering data was successful with a globular architecture for the aggregates and coil behavior for nonattached linear chains. The analysis gave evidence to clustering of segments. A large number of the linear mass density was found combined with a considerable chain stiffness. Indications were found that the fraction of free chains was overestimated. A significant part of the chains appeared to be attached to the aggregates. Sterical stabilization in the course of dissolution of the glassy material, combined with hydrogen bonding, are suggested as the reason for the incomplete dissolution.

Introduction

In a previous paper 1,[1] we reported the synthesis and the global properties of poly(*N*-vinylimidazole) (PVI) in ethanol. Common flexible chain behavior was found in the low molar mass regime. However, for the samples of high molar mass a peculiar behavior was found with an unexpected break in behavior around a molar mass $M_w = 8 \times 10^5$ g/mol which was accompanied by a striking increase in the radius of gyration R_g by a factor of 3. A very weak further increase of R_g with the molar particle mass was obtained. Simultaneously, a decrease in the intrinsic viscosity and the second virial coefficient was observed. The result was interpreted by the formation of aggregates. A number of questions remained open which could not be answered with the measured global parameters. Additional information from other measurements appeared to be necessary. Besides the yet not understood occurrence of the break point, below that molecular dispersity was obtained, the very surprising properties of the aggregates aroused our interest to learn more of the aggregate structure. A suitable approach is offered by a detailed analysis of the angular envelope of the scattered light. The molecularly dissolved samples of $M_w < 8 \times 10^5$ g/mol were not very informative. The angular dependence gave just a set of parallel straight lines in the Zimm plot which was expected for flexible coils of single linear chains.

However, in the high molar mass regime of $M_w > 8 \times 10^5$ g/mol the radii of gyration were larger than 100 nm, which with the wavelength λ of the used light gave values of $qR_g > 2$ ($q = (4\pi/\lambda) \sin(\theta/2)$). In this region not only the global property of the radius of gyration or the hydrodynamic radius can be measured but also some details on the internal structure are probed. To get a deeper insight into the aggregate structure, we carried out a detailed curve analysis of the angular dependence from the high molar mass PVI particles. The results are discussed on the basis of well-studied models which were taken as a framework for a classification of the present aggregates.

Mostly the systems are considered as an ensemble of homologous structures, for instance as a system of uniform or polydisperse spheres or rigid rods of different radius or length, respectively, to mention here only two examples among many others. Homogeneity in architecture is also present in a system of randomly cross-linked flexible linear chains.[2] Such systems are easily characterized on the basis of well-developed theories.[2−6] Changes in homogeneity also become likely when the aggregation causes restriction in the segmental mobility. Such polymer one-component systems in a solvent are the first type of models in our consideration. Often, however, these systems have a heterogeneous structure. Best known is the wormlike chain model by Kratky and Porod[7] which displays random coil behavior at small q values (low scattering angle) but rigid-rod behavior at large q values, corresponding to short distances in the chain.

Other model types consist of a system in which nonassociated chains and aggregated chains coexist in the solution. In this case an attempt has to be made to separate these two components. To some extent, a selective precipitation could give valuable information, but a complete separation was not possible also with other sytems[8] and cannot be expected on the basis of common fractionation theories.[9,10] In any case the high concentration phase after partial precipitation always contains a certain amount of short chains, and vice versa, the dilute phase contains a small fraction of high molar mass particles. Another way of separation consists of a mathematical analysis of the scattering curves

[†] Albert-Ludwig-University Freiburg.
[‡] "Transilvania" University of Brasov.
* Corresponding author: e-mail walther.burchard@makro.uni-freiburg.de.

10.1021/ma0353639 CCC: $27.50
Published on Web 03/24/2004

from such a two-component system.[11−14] However, if linear chains are attached to the first component and are not independently moving, differentiation between the two possibilities of attached or free chains will be difficult or may not even be feasible without data from other independent measurements. Separation of the two components is commonly achieved by size exclusion chromatography. In the present case, however, the aggreated particles of poly(vinylimidazole) were too large. They were filtered off by the gel and finally blocked the flow.

The main difficulties in the description of aggregates, in particular of a polymer two-component system, arise from the fact that the architecture of the aggregates is not known, and this problem becomes further involved by a large size distribution. Several research groups, including us,[11−14] employed an empirical procedure for mathematical separation of the two components. Such a treatment requires reasonable assumptions on the architecture of the high molar mass aggregate component and mostly also of the other component. For instance, equivalence in structure of randomly branched polymers with randomly associated particles is often assumed. Such structures may be similar to the observed high molar mass particles, also with regards of polydispersity. A very informative study was previously made with molecularly dispersed starches which contained the linear amylose ($M_w < 10^6$ g/mol) in coexistence with very large and highly branched amylopectin molecules ($M_w = 70 \times 10^6$ g/mol).[15] A complete and very satisfying analysis of the scattering curve became possible because the amylose content was separately determined by potentiometry. Also, the structure of amylopectin was approximately known from studies with waxy maize starch that solely consists of amylopectin. Two important observations were made. (i) The large component strongly governed the scattering behavior and dominated the initial regime of small scattering angles. The measured *z*-average mean-square radius of gyration almost entirely represented the radius of the large M_w component. (ii) The segmental mobility in the large amylopectin component was reduced by the high segment density due to branching, and this effect became drastically enhanced in the semidilute concentration regime.[16−19]

In the present paper a curve analysis is carried out of the q dependencies in static light scattering from the high-M_w PVI particles above the break point in the global properties at $M_w = 8 \times 10^5$ g/mol.[1] Compared to the low-M_w chains, the high-M_w particles displayed strikingly unusual behavior in static and dynamic light scattering and gave evidence to a marked heterogeneity in size and internal structure. The highly complex behavior of the dynamic light scattering data will be presented separately in a forthcoming paper.[20]

Theory

Static Light Scattering. Some basic relationships of static light scattering (SLS) have already been outlined in the previous paper 1[1] and will not be repeated. However, there are some new aspects which have to be kept in mind.

(i) For homologous systems of *self-similar objects* the particle scattering factor $P(u) = i(\theta)/i(\theta = 0)$ is a *unique* function of the parameter $u = qR_g$,[2] where $q = (4\pi n_0/\lambda_0)\sin(\theta/2)$ with λ_0 the wavelength of the light in a vacuum, n_0 the solvent refractive index, and θ the scattering angle. For materials of the same architecture this universality of the two quantities permits representation of scattering data from samples of different molar mass in one common graph. The obtained curves are identical with those obtained with one selected sample but measured at different wavelengths. The results from small-angle neutron (SANS) and small-angle X-ray (SAXS) scattering likewise can be used.

(ii) Differences in architecture become detectable only in the far q-region where $qR_g > 2$. However, in that region the scattering intensity has already decayed to very low values, which makes a distinction between the various architectures difficult and inaccurate. Therefore, all of the present results will be represented in normalized Kratky plots[21] in which the particle scattering factor $P(u)$ is multiplied by u^2. The advantage of the Kratky plot is that the asymptotic part at large u values is strongly amplified (by factors u^2), and this makes differences more easily discernible than in the mostly applied double-logarithmic presentation. In some cases, when rodlike particles are presumed being present in the system, the so-called Casassa−Holtzer plot[22,23] is preferred, in which the data of $(q/\pi)M_wP(q)$ are plotted against u. The latter procedure is not as sensitive as the Kratky plot but permits the determination of the linear mass density $M_L = M_w/L_w$, which is a valuable structure quantity, for instance when several chains may be aligned side-by-side to form a thin cylinder over a certain length. Both plots will be applied to the data from the PVI aggregates. The *Kratky and Casassa−Holtzer plots need no assumptions* and only represent the experimental data as measured in another way. L_w is the contour length of chains which for aggregates will be defined below.

Mostly, the analysis on the basis of well-known theoretically derived particle scattering factors is successful if the polymer system consists of only one type of architecture. If the system comprises two species of different architecture, ambiguity arises and causes problems. Information from other types of measurements and theoretically studied model have to be taken into account. Despite these problems, a certain classification within a framework still became possible.

Remarks on a Two-Component System. For a two-component system quite generally the following three relationships hold

$$P_z(u) = aP_1(u_1) + (1 - a)P_2(u_2) \tag{1}$$

$$a = \frac{mM_{w1}}{M_w} \quad \text{and} \quad 1 - a = \frac{(1 - m)M_{w2}}{M_w} \tag{2}$$

$$u^2 = q^2R_g{}^2 = aq^2R_{g1}{}^2 + (1 - a)q^2R_{g2}{}^2 \tag{3}$$

with m the mass fraction of the aggregate component. The subscripts z denotes the z-averages and the indices 1 and 2 refer to the high (aggregate) and low molar mass (single chains) components. In these coupled equations the root-mean-square radius $\langle S^2\rangle_z{}^{1/2} \equiv R_g$, the weight-average molar mass M_w, and the z-average particles scattering factor $P_z(qR_g)$ are known from the experiment. Unknown and to be found from a curve analysis are the radii of gyration R_{g1} and R_{g2}, the molar masses M_{w1} and M_{w2}, the shape of the particle scattering factors $P_1(q)$ and $P_2(q)$ of the two components, and finally the amplitude a. The analysis is facilitated by the already mentioned fact that the radius of gyration of the large

aggregate component is very close the measured radius of gyration, i.e., $R_{g1} \approx R_g$. Furthermore, the low molar mass component can often be assumed to be small such that $u_2 < 1.2$. Under this condition there is no significant difference in the angular dependence between the various architectures. Therefore, the particles scattering factor of the low molar mass component can approximately be described by the simple Zimm equation,[24] which is universal for any structure if $qR_g < 1.2$

$$1/P_2(u) \cong 1 + u_2^2/3 + ... \quad (4)$$

To proceed further, one has to make an assumption on the particle scattering factor for the aggregated particles. Some information can be taken from the measurements of the global properties. For instance, the value of the $\rho = R_g/R_h$ parameter, which was reported in paper 1, gives a hint. The observed small values obtained from the measurements of the high molar mass PVI particles indicated a contracted structure. A value larger than $\rho = 2$ would be a sign for expanded, fairly stiff objects, but values around $\rho \approx 0.6$ are characteristic of microgels. As was shown by Guinier,[25,26] the following approximation serves as a very efficient starting point for globular structures

$$P_1(u_1) \cong \exp(-u_1^2/3) \quad (5)$$

Note at small u_1^2 values eq 4 is recovered. For the low molar mass component a stiff chain behavior may be present. The particle scattering factor of a polydisperse rigid rod is given by the equation[27]

$$P_{1,rod}(u_2) \cong (1/u_2) \arctan(u_2) \quad (6)$$

The assumption of eq 6 will be an unsuitable choice for semiflexible chains; the theory of wormlike chains by Koyama should be used,[28,29] but the corresponding complex relationship could not yet be incorporated in our nonlinear fit procedure. A best fit has to be found by nonlinear regression for the unknown parameters a, R_{g1}, and R_{g2}. The fit of the angular dependence with eq 1 has to be repeated until the constraint of eq 3 is fulfilled, which mostly requires only a minor change of the parameters. The choice of the function type for $P_1(u_1)$ and $P_2(u_2)$ may have to be varied according to experience with well-studied models and by trial-and-error to receive the best representation of the measured scattering curve. If the molar mass of one of the two components could be estimated from other sources, also the mass fraction m of aggregated particles can be obtained from the coefficient a. For instance, with a known M_{w2} of nonaggregeted chains eq 2 yields

$$m = 1 - \frac{(1 - a)M_w}{M_{w2}} \quad (7)$$

Results

The structural investigation of PVI solutions was started as usual with the evaluation of Zimm plots.[24] Straight lines were obtained for low molar masses ($M_w < 8 \times 10^5$ g/mol), indicating the presence of nonaggregated linear random coils (see paper 1). However, in the high molar masses region of aggregated particles ($M_w > 8 \times 10^5$ g/mol), the angular dependence exhibited very striking features even in the Guinier modification of the Zimm plot, with a steep initial part at low scattering angles and a flatter curve at large scattering angles. One example is shown in Figure 1. The steep initial part is characteristic of very large particles. This could be caused by a supramolecular structure being present besides the molecularly dispersed chains. However, as outlined in the theoretical section, a similar shape of the angular dependent scattering curve also could have it origin in a one-component aggregate structure with a heterogeneous internal architecture.

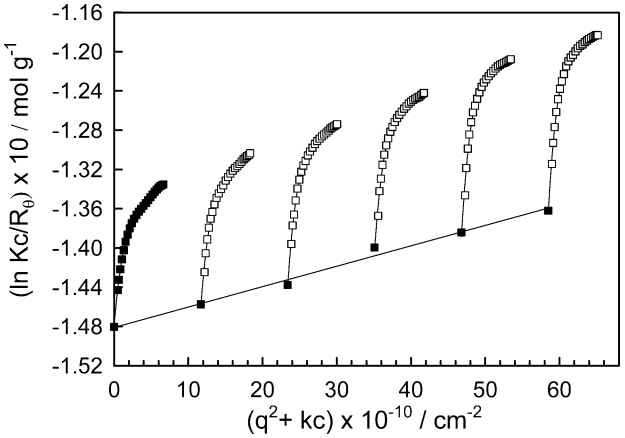

Figure 1. Modified Guinier plot ($\ln(Kc/R_\theta)$ vs $q^2 + kc$) of PVID in ethanol. $M_w = 2.69 \times 10^6$ g/mol, $R_g = 164$ nm, $A_2 = 2.26 \times 10^{-5}$ mol mL/g^2. Measurements were made in steps of 5° in a range from 30° to 145°. The full lines are fit curves with a polynomial of fifth order. The well-developed linear initial slope were obtained with the first eight angles and a second-order polynomial fit. The well-defined initial linear part guaranteed accurate determination of the radius of gyration. Besides the serial fits of each concentration a simultaneous fit of the whole data set was made denominated as a *smooth* routine.

The steep initial part in Figure 1 is primarily caused by the shape of a high molar mass that has a globular structure. The flat curve at large angles, on the other hand, arises from short chain sections, which could be covalently linked to the large particles but also could originate from nonattached linear chains. In the first approach we compared our experimental curves with one-component particle systems, i.e., linear wormlike chains,[28−30] star-branched particles with semiflexible chains,[31] and the soft sphere model.[32] This approach permitted a rather satisfying classification. We then continued with a two-component analysis where well-defined special structure models were considered.

One-Component Aggregate Systems. Originally, the Kratky plot[7,21] was developed for the one-component system of wormlike linear chains. Two different aspects of the architecture have to be underlined. Figure 2 gives a schematic representation of the model. At small qR_g values the whole particles are seen in the scattering experiment comprising a large number of Kuhn segments. In this regime the chain resembles a common random coil. At large qR_g values, however, only short sections of the particles are probed, and rodlike behavior will be observed if only the length scale of one Kuhn segment is probed. Both aspects become noticeable when a large domain of qR_g values is covered.

Figure 3 shows the Kratky plots for the five nonfractionated PVI particles of high molar mass. Two main effects are clearly recognized from this figure. (i) The scattering curves from the five samples do not coincide. This behavior reminds of the soft sphere model[32] that is shown in Figure 4 with examples of various branching

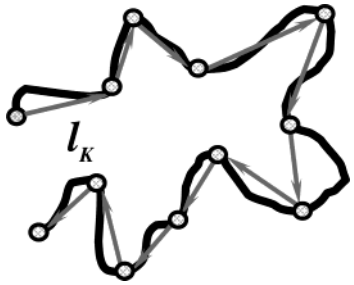

Figure 2. Model of semiflexible wormlike chain (full line). The lengths of the vectors represent the Kuhn segment lengths (l_K). The open circles correspond to the beads in the spring−bead model. The wormlike chain combines common Gaussian behavior at small q values (long distances in space) and rodlike behavior at large q values (short distances in space) and is the simplest example of a one-component heterogeneous structure.

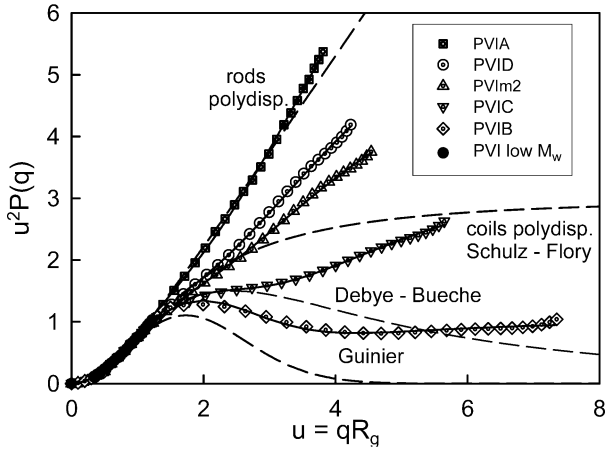

Figure 3. Kratky plots $(qR_g)^2P(qR_g)$ vs qR_g of the experimental particle scattering functions, $P(qR_g) = R_\theta/R_{\theta=0}$, from low and high PVI molar masses. The fit curves from the Guinier plots are shown as solid lines through the data points. For comparison, some theoretically curves of simple macromolecular one-component structures were added (dashed lines). The Guinier approximation very satisfactorily describes the initial part of the curves up to $u = qR_g = 1.2$.

generations. This model describes generalized dendrimers in which the branching points are connected via spacers of Gaussian chains. The degree of polymerization of the spacer was chosen DP = 7500, which is slightly smaller than the chain length of single PVI chains at the break point. A globular structure is well developed for generations $n > 3$. Simultaneously, the property of linear flexible chains becomes apparent if $u > 4$. The spacer chains are in the unperturbed conformation which are characterized by a fractal dimension of $d_f = 2$.[6,33] In the Kratky representation this chain behavior is equivalent to a q-independent plateau. Figure 4 also demonstrates the excellent validity of he Guinier approximation in the region up to $u = 4$, if the number of generations is larger than $n = 5$. For comparison, the experimental data points from the PVIB sample are added. (ii) At large $u = qR_g$ the curves do not approach a plateau as expected for a random coil in a poor solvent but show an approximately linear increase. This reminds one of star-branched objects of increasing number of arms in which the arms are semiflexible[31] (Figure 5).

The asymptotic increase at large u could have its origin in two effects. The one is the influence of a strong excluded-volume interaction,[34] and the other could arise

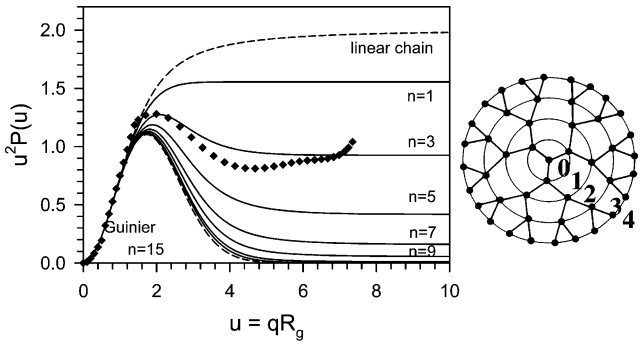

Figure 4. Theoretical scattering behavior of the soft sphere model[32] for various generations. The soft sphere model represents generalized dendrimers in which the various generations are connected via long chain spacers which are in the unperturbed state. For comparison, the experimental data from the sample PVIB are added. The increase at large u values results from chain stiffness of the spacer chains (compare Figure 5). The last four points are cause by back-reflection of the primary beam on the surface of the outgoing glass window of the scattering cell because there is a significant difference in the refractive index between ethanol and glass. Note: at generation number 1 the soft sphere coincides with the well-known 3-arm star molecule.

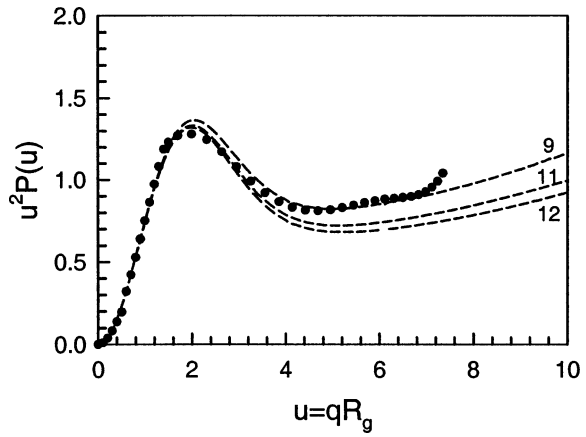

Figure 5. Kratky plots derived from the theory of scattering from star-branched macromolecules with monodisperse wormlike arms.[31] The filled symbols represent the experimental data from PVIB. The dashed curves were calculated for arm numbers of 9, 11, and 12 with arm lengths of $DP_{arm} = 7500$, a value that corresponds to PVI chains shortly below the break where aggregates were observed.

from a certain chain stiffness.[28−30] The former possibility can be ruled out because PVI in ethanol exhibited typical marginal solution behavior.[1] In other words, only a weak excluded volume is effective.

Nonbranched Wormlike Chains. For linear chains the stiffness can be analyzed qualitatively and quantitatively on the basis of the Kratky−Porod model (Figure 2) and, more accurately, by the theory of Koyama.[28] In the Kratky−Porod procedure a kink point q^* is evaluated, i.e., the point where the asymptotic straight line intersects the curve of the coil, which for a Gaussian coil shows a q-independent plateau. At this point the particle scattering factor of a rod has the same value as that of a coil of the same contour length L. This characteristic point is related to the Kuhn segment length l_K by the equation

$$q^* = \frac{12}{\pi}\frac{1}{l_K} \quad \text{or} \quad l_K = 3.82/q^* \tag{8}$$

Table 1. Results Obtained from Evaluations of the Kratky Plots[a]

sample	$M_w \times 10^{-5}$ (g/mol)	R_g (nm)	u^*	l^*_{rod} (nm)	q^* (nm^{-1})	l_K (nm)
PVIA	8.0	150				
PVID	26.9	164	1.85	89	0.011 28	339
PVIm2	36.6	176	1.91	92	0.010 85	352
PVIC	85.7	219	2.92	75	0.013 33	287
PVIB	586.0	285	3.70	77	0.013 0	293

[a] u^* is the kink point, $l^*_{rod} = R_g/u^*$ corresponds to the rod length that became dominating, $q^* = u^*/R_g$, and $l_K = 3.82/q^*$ is the Kuhn segment length only for linear chains. For branched and more complex heterogeneous structures the relationship between q^* and the persistence length is not yet known.

The relation becomes *inaccurate* and even wrong if the mentioned plateau is not obtained or when a maximum occurs resulting from a *more compact* particles than the random coil. In Figure 3 the intersection points of the five curves appear at different $u^* = q^*R_g$ values. This fact has its origin in the ratio of stiff chain segment lengths to the value of radius of gyration. The intersection is shifted more and more to smaller values if the stiff chain segment lengths come into the range of the radius of gyration of the whole macromolecule. With two of the five PVI aggregated samples the intersection point could clearly be determined, in two other ones the estimation became somewhat uncertain, and for the PVIA particles the Kratky curve seemed fully to be governed by a rodlike structure, for which a linear increase with u^2 is predicted (for more details see below). For linear wormlike chains no maximum is obtained, and the asypmtotic plateau height is $u^2P(u) = 2$ for monodisperse chain and 3 for polydisperse chains of the most probable distribution. With increasing chain stiffness the asymptotic linear increase is shifted toward smaller u values, and for chains less than 4 Kuhn segments in length the mentioned plateau no longer is reached. The values of u^* are listed in Table 1 together with the values of $R_g/u^* = l^*$ rod, where the latter gives an impression on the length of a chain that visibly contributes to the scattering curve. Calculation of Kuhn segments on the basis of eq 8 gave segment lengths larger than the radii of gyration. The behavior can only be obtained if the chain is almost a rigid rod (for polydisperse rods one has $R_g = L_w/2$). Such large Kuhn segments are not likely. In fact, application of eq 8 is no longer justified when the scattering curves in the Kratky representation pass through a maximum before the observed kink in behavior occurs. Furthermore, the best fit with the Koyama relationship for the angular dependence resulted in a curve that fully neglects the observed maximum. Evidently, the aggregated PVI particles cannot be described by a linear wormlike chain or cylinder.

Linear Mass Density. Details on a rodlike structure in the far u-region can be obtained from the Casassa−Holzer plot, which is shown in Figure 6 for the five samples. The particle scattering factor of a rod decreases in the asymptotic region as $P(q) \sim \pi/(qL)$.[25] Thus, a plot of $(q/\pi)M_wP(q)$ should give a q-independent plateau whose value is $M_w/L_w \equiv M_L$, the mass per unit length or linear mass density. This result from theory has been realized by SANS or SAXS in many cases.[35,36]

In a theoretical and experimental study Herzog et al.[37] demonstrated that this relationship remains valid for any architecture that is built up of linear subchains. For sufficiently short sections all these chains approach

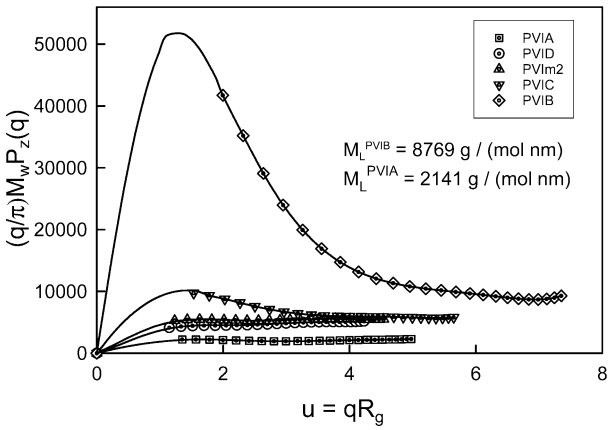

Figure 6. Casassa−Holtzer plot from the high molar mass PVI particles. The plateau height gives the linear mass density $M_L = M_w/L_w$.[7,35] The relationship was first derived for linear chains but remains valid for all structures which are built up of chains[37] (see Figure 7). For linear stiff chains the ratio of the maximum height to that of the plateau increases with the number N_K of Kuhn segments in a semiflexible rod[29] (Figure 13). For generalized structures the corresponding relationships are not yet known. The symbol M_w refers to the molar mass of particles, not of single chain molecules. The weight-average contour length L_w represents a generalized primitive contour length as demonstrated in Figure 7.

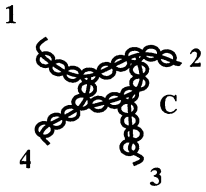

Figure 7. Example of a generalized macromolecular structure. The generalized contour length L is given by the sum over all contour lengths of subchains.[37] In the present example one has $L = L_1 + L_2 + L_3 + L_4 + C$, where C represents the cycle length and the L_j the lengths of the chains starting at the cycle. The open symbols need not be simple monomer repeat units but can consist of aggregated segments or small globules. In these case the solid lines through the centers of he beads have to be taken ("primitive" contour length).

rodlike behavior, usually expressed in terms of Kuhn segments l_K or persistence length $l_P = l_K/2$. In a general architecture the contour length L is the sum of all contour lengths from dangling chains and from chains which connect two branching points. Also cycles are included in this sum. Figure 7 demonstrates what is meant. It is important to realize that the units (represented in Figure 7 by beads) need not be the repeating unit of a single macromolecular chain, but these units could consist of any structure, say blobs in de Gennes' notation,[38] or microphase-separated small globules, which not perfectly need be of the same size. In other words, the term linear chain section actually means a *primitive* linear chain as is indicated by the solid lines in Figure 7. The plot of $(q/\pi)P(q)$ will asymptotically approach for all these structures a plateau at sufficiently large u values. The height of this plateau gives the generalized reciprocal contour length. When this function is multiplied by the molar mass of the particle the linear mass density $M_L^{exp} = M_w/L_w$[35,36] is obtained. This quantity is another important structure parameter that is obtained experimentally *without assumptions*.

The data are shown in column 3 of Table 2. The linear mass density of a single PVI chain can be calculated from the monomer bond length $l_0 = 0.25$ nm and the

Table 2. Results Obtained from Evaluations of the Casassa−Holtzer Plots[a]

sample	$M_w \times 10^{-5}$ (g/mol)	M/L (g/(mol nm))	n_{agg}	L (nm)	u_{max}
PVIA	8.0	2142	5.8	373	1.57
PVID	26.9	5135	14.0	524	1.66
PVIm2	36.6	5426	14.7	675	1.63
PVIC	85.7	5672	15.4	1511	1.39
PVIB	586.0	8769	23.8	6683	1.20

[a] n_{agg} is the number of laterally packed monomer units in a short rodlike section, L is the generalized contour length (see Figure 7), u_{max} is the position of the maximum, and M_w is the molar mass of particles, not of single chains.

molar mass of the monomer M_0 which gives $M_{L1} = M_0/l_0 = 368$ g/(mol nm), where the subscript L1 denotes the linear mass density of single, nonassociated chains. With this value the number of side-by-side aligned chain sections or otherwise aggregated units is obtained as $n_{agg} = M_L/M_{L1}$, and the generalized contour length L_w is derived from M_w and M_L according to $L_w = M_w/M_L$. Semiflexible chains develop in the Casassa−Holtzer representation a *maximum at a position* of $u_{max} = 1.43$ for uniform chain which with increasing polydispersity is shifted by a factor $(M_z/M_w)^{1/2}$ toward higher values and occurs for $M_w/M_n = 2$ at $u_{max} = 1.73$. Therefore, the actually observed u_{max} position permits for linear chains a rough estimation of the polydispersity. The correlation of the maximum position to the particle architecture has not yet systematically been investigated. For star-branched macromolecules and the soft sphere model a clear shift toward smaller u values occurs when the number of arms in the star or generation in the soft sphere model is increased. In any case, the position is a characteristic structure parameter. The experimental values of u_{max} from the five PVI samples are given in the last column of Table 2. Also the *height of the maximum* is a structure sensitive parameter. For linear chains the ratio of the height to the plateau height is a measure of the number N_K of Kuhn segments per contour length which was calculated by Schmidt et al.[29] for a series of N_K. Figure 13 shows the correlation of the maximum to the plateau heights (M/P) and the least-squares fit results of this dependence. The curve reaches the asymptotic of $M/P = (3/2)(2N_K)^{1/2}$ at about $N_K > 300$, which already represent Gaussian chains in a good approximation. For linear chains this relationship is of great value as it allows us to find the Kuhn segment length $l_K = L/N_K$. However, this relationship is no longer valid if branched structures occur. We skip a discussion of the evaluated data which gave far too large l_K values as could be expected, since our PVI particles had clear globular characteristics. (In this paper branching and ring formation do not mean covalent linkages.)

Attached Chains to a Globular Core (Star-Branched Microgels). Two limiting cases may be considered. In the first the core is small to the wavelength of the light and can be considered as a pointlike scatterer. Also, its weight will be negligible compared to the measured molar particle mass. Typical synthetically prepared examples were studied by Lang et al.[39] The synthetically prepared structure (with covalent bonds) and that of the PVI particles (physical bond) resemble star-branched macromolecules with semiflexible rays (Figure 5). This model was analytically calculated by Huber and Burchard[31] in a combinatorial approximation. Indeed, the derived Kratky plots for the particle scattering factors, showed much similarity with our experimentally observed curve. The Huber and Burchard predicted behavior result was confirmed by Brownian simulations for 12-arm polystyrene stars by Freire et al.[40] The weak increase of the scattering curve in the far q-region, as was observed also by Richter et al.[34] was mostly interpreted in the literature as a result of excluded-volume interaction. This is at variance with the specific analytical theory by Allegra and Ganazzoli,[41−44] who still obtained a continuous decrease in the asymptotic region of u. Earlier simulation for polystyrene 12-arm stars by Huber et al.[45] on Flory's model of rotatory isomeric states (RIS model)[46] clearly demonstrated that the experimentally observed increase in the Kratky asymptote arose from chain stiffness of the polystyrene arms.

Figure 8. Star-branched microgel (shaded core) with semiflexible rays.[39]

However, the initial part of the scattering curves from the PVI aggregates is fully determined by a marked globular structure on which the attached linear chains have no influence. This structure has more similarities to microgels with dangling arms (Figure 8) or core−shell structures, in which the globular structure of the extended core contribute even more. This is clearly demonstrated with the soft sphere-model of Figure 4, for which a possible chain stiffness was not yet taken into account. Now the weight fraction of this central core is in the order of the corresponding weight from the sum of all dangling chains. Monodisperse microgels were prepared in a previous study by Nerger et al.[47] by cross-linking polymerization in narrowly distributed latex particles. After polymerization the stabilizing surfactant was removed whereupon the particles became soluble in a organic solvent. The angular dependence of the scattered light from these particles could described by the soft sphere model.[32] This model would be in good agreement with the experimental observation when the chain stiffness is introduced. The corresponding calculations are tedious but seem to be possible. The corresponding calculations are in progress.

Two Polymer Component Systems. Now we come to the other alternative that the aggregated system consisted of two components of different size and structure, i.e., of nonassociated chains and highly aggregated globular particles. As already mentioned in the beginning of the paper and demonstrated in Figure 1 and Figure 3, the initial part of the scattering curve could be well described by the Guinier approximation.[25] This globular form factor was successful for a fit of all five large PVI samples at small to intermediate u values, but at large u values the scattering curves revealed very different behavior in the Kratky plot (Figure 3). The PVI macromolecules with $M_w < 8 \times 10^5$ g/mol had small R_g values and are all in the region of $qR_g < 2$. Only the radius of gyration could be determined in this range. The shape from all these curves could be described by Zimm's eq 3 with no deviation from each

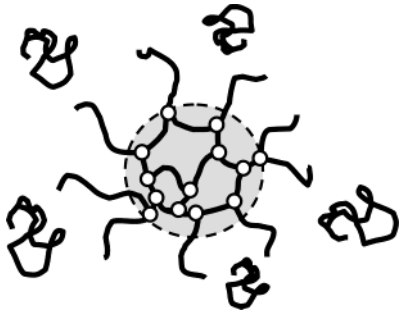

Figure 9. Swollen microgel with dangling chains in coexistence with nonattached coils of individual chains. The internal segments between branching points may possess chain stiffness. The dangling chains in the corona cause a steric stabilization and prevent phase separation. The stabilization also holds true for noncovalent bonds (e.g., hydrogen bonds) in the microgels. Because of polydispersity the structures do not present common core−shell structures.

other. A discrimination of various conformations with these samples was not possible. However, the much larger dimensions of the PVI particles with $M_w > 8 \times 10^5$ g/mol covered the structure-significant region of $u = qR_g > 2$. In a polymer two-component system the probed short distances comprise segments inside of the large particles but also nonattached linear chains.

In the two-component analysis we chose as already outlined the Guinier approximation for the large particles of high molar mass and the Zimm particle scattering factor for the nonattached linear flexible chains. This choice is a well-founded procedure. In most SANS experiments the Guinier approximation is used as the only fit to find the radius of gyration, and this routine is employed even to flexible chains, where it is a rather poor approximation. Also, the two-component fit, or deconvolution, is familiar in SANS interpretation. In the Kratky representation the total *z*-average particle scattering factor is given by the equation[48,49]

$$u^2P(q) = u^2\left[a\,\exp(-bq^2) + (1-a)\frac{1}{1+cq^2}\right] \quad (9)$$

in which the three parameters a, b, and c are fit parameters. These three parameters are related to the molar masses and the radii of gyration of the two components as given by the relationships of eq 2 with

$$b = {R_{g1}}^2/3 \qquad c = {R_{g2}}^2/3 \quad (10)$$

and u is related to these quantities as given by eq 3.

We performed the curve analysis with common nonlinear regression programs for flexible and for rodlike linear chains in the second, nonassociated component. Only for flexible chains a satisfactory fit was possible. The rigid-rod model failed to describe the small component behavior, although the Kratky plot seemed to suggest it. Figures 9 and 10 demonstrate the fits for two examples, with the flexible and the rodlike chain models for the low molar mass components. The individual components and their sum are shown separately by dash and point-dash lines. The findings are not really unexpected because a rigid-rod approximation is certainly poor for nonattached semiflexible chains. Because of the complex mathematical structure of the Koyama equations,[28] we have not yet been able to incorporate the model in our fit procedure. If these chains are short,

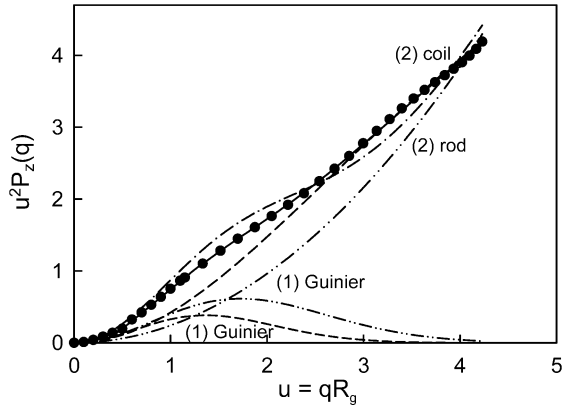

Figure 10. Two-component curve analysis (deconvolutions) demonstrated with PVID. The experimental curve (symbols) resemble rigid chain behavior. However, the curve could be well described by a two-component linear regression fit with flexible linear chains as the small component and globular aggregates. A corresponding fit with rigid-rod behavior for the short component failed. The globular component was represented by the Guinier approximation. The full line represents the fit with flexible linear chains and the dashed lines those of the individual components. The corresponding curves with rigid rods as the small components are represented by the dash-point curves.

differences between a random coil and a semiflexible chain will not be detectable.

Mass Fractions of the Two Components. From the described nonlinear regression fits the weight fractions a and $(1 - a)$ and the radii of gyration of the two components were determined. To find the mass fractions of these components, an *assumption* had to be made. We assumed that the low molar mass component exclusively consisted of nonattached linear chains, and these should have the same conformational characteristics as the molecularly dispersed chains in the range of $M_w < 8 \times 10^5$ g/mol. Actually, the first part of this assumption corresponds to a limit because to some extent the chains also could be attached to the aggregate. The second part appeared to us sensible because there is no reason that the nonattached chains should show behavior different from those without large particles in the system. For these chains the molar mass dependence of the radius of gyration was determined in the previous paper, which followed the relationship

$$R_g = 0.0483{M_w}^{0.53}\ \text{nm} \quad (11)$$

Since the radius R_{g2} is known from the curve analysis now the molar mass M_{w2} could be estimated. Making use of eq 7 the mass fraction is the obtained

$$m = 1 - \frac{(1-a)M_w}{M_{w2}} \quad (7)$$

and subsequently the molar mass M_{w1} of the aggregates

$$M_{w1} = \frac{M_w - (1-m)M_{w2}}{m} \quad (12)$$

The data are collected in Table 3.

Discussion

The discussion will be divided into three significant different sections. The first one will recall the experimental observation made in the study of previous and

Table 3. Weight Average of Molar Masses M_w and Radii of Gyration R_g of Molecularly Dissolved PVI Chains with $M_w < 8 \times 10^5$ g/mol[a]

PVI			large component (aggregated particles)				small component (linear chains)	
sample	$M_w \times 10^{-5}$ (g/mol)	R_g (nm)	a (%)	m_1 (%)	$M_{w1} \times 10^{-5}$ (g/mol)	R_{g1} (nm)	$M_{w2} \times 10^{-5}$ (g/mol)	R_{g2} (nm)
PVIA	8	150	46.5	39	9	190	7	46
PVID	26.9	164	56	12	125	208	13	63
PVIm2	36.6	176	58	25	85	220	20	77
PVIC	85.7	219	78.5	30	222	228	26	87
PVIB	586	285	85	30	1660	277	125	183

[a] M_{w1} and M_{w2} are the molar masses of aggregates and linear chains, and R_{g1} and R_{g2} are the corresponding radii of gyration. a is the weight fraction of the large aggregates and was determined by fits.

the present paper where *no* assumptions were made. The list of striking phenomena disclosed properties which markedly differ from those of linear molecularly dispersed polymers. These facts present a troublesome challenge to everybody who wishes to find out essential features of aggregated structures. This challenge is taken up in the second part. We tried to extract logically consistent conclusions. Not all questions could be answered in this manner. We thus added in the third part a personal view, which at present only can have the character of a hypothesis. Nonetheless, we decided to add this view because we have the hope that this will provoke new ideas, which in turn may initiate colleagues, and ourselves, to carry out new model calculations.

Experimental Facts. (1) Common molecularly dispersed solution behavior was found for PVI of low molar mass. Around a molar mass of $M_w = 8 \times 10^5$ g/mol a break in the solution properties of PVI in absolute ethanol was observed. For higher molar masses than this break point the radius strongly increased by a factor of 3. (2) The same break was observed with the hydrodynamic radius R_h, the second virial coefficient A_2, and the intrinsic viscosity $[\eta]$. While the two radii R_h and R_g *increased* shortly after the break point, the second virial coefficient and the intrinsic viscosity *decreased*. (3) Power law behavior was found in the two regimes below an above the break point but with different exponents. The exponents in the low molar mass regime corresponded to the familiar fractal behavior of nonassociated flexible linear chains in a marginally good solvent. In the high-M_w regime, however, the exponents violate the scaling relationships among the various exponents and are no longer related to a fractal dimension. These samples are to be considered as aggregates from linear chains that was concluded from the following observations. (4) Contrary to the behavior of common linear chains, the apparent segment density strongly increased after the break point whereas below the break point the expected common decrease was found. (5) The angular dependence of scattered light showed in the range of $u < 2$ typical behavior of globular structures. This part has universal character and is well represented by the Guinier approximation. (6) At values of $u > 2$ characteristic deviations occurred. The deviations were especially clearly seen for the highest molar mass particle. With the sample close the break point the deviations started to dominate the global properties. (7) Kratky and Casassa−Holtzer plots are different forms of representing experimental data and emphasize special features of the angular dependence of the scattered light, which are related to structure specific parameters. The kink points in the Kratky plots which marked the deviation from global structure occurred at u^* values between 1.85 and 3.70 and describe a length scale of $l^* = u^*/R_g$, which was in the fairly narrow range of 77−92 nm. (8) The Casassa−Holtzer plot includes the molar mass and permitted the estimation of a contour length L and a linear mass density $M_L^{exp} = M_w/L_w$. The contour length was shown by theory and experiment to be the sum of the contour length of all dangling chains and of the subchains connecting two branching pionts in the particle. (9) The experimental values of M_L^{exp} increased with the molar mass of the particles and varied between $5.8M_{L1}$ and $23.8M_{L1}$, where $M_{L1} = M_{mon}/l_{mon}$ is the linear mass density of a single, nonassociated PVI chain. (10) Position and height of the maxima in the Casassa−Holtzer plots varied with the molar mass of the particles.

One-Component Particle Structure in Solution. This consideration refers to the one limit in our structure classification, and the question has to be checked as to what extent the extracted structure parameters give a reasonable answer. Clearly the aggregates must be heterogeneous in structure consisting of an overall globular shape but with rigid segment sections. Otherwise, the large radii of gyration of the particles cannot be explained and not be simulated with already known models. Branching and aggregation cause a decrease of the radii (g-contraction factor[50]). On the other hand, polydispersity causes an increase of the z-average mean-square radius of gyration. The two effects, branching and polydispersity, largely balance each other. Even for the broadest size distribution of randomly branched macromolecules (with $M_w/M_n > 100$) the increase in $R_{g,branch}$ is $R_{g,branch}/R_{g,lin} = 2^{1/2}$ for the branched chain compared to the linear one of the same weight-average molar mass.[5,51]

The data of $n_{agg} = M_L^{exp}/M_{L1}$ suggest that the stiffening is correlated to n_{agg}. The arrangement of the PVI monomer units in the segments is not known. It could consist of microphase separated small globules, but there may well be some order in the arrangement. It was certainly a great discovery by Rees[52] and his opponent Smidsroed[53] that the observed M_L values, in all linear polysaccharides, many filamentous proteins and DNA molecules, originated from side-by-side alignment of segments, at least over a certain length (junction zone formation). Often double and triple helices were realized,[54−56] but in numerous other examples no intertwining was effective. We do not insist on this model of junction zone formation but still keep it as one among several other possibilities. One point, however, remains clear: if the domains consist of large globules, say $> \lambda/20$, no plateau can occur in the Casassa−Holtzer plot. *Only rigid linear segments can produce such constant plateau in the asymptotic region*. For all other sub-macromolecular structures a continuous decrease to zero takes place.

It is unlikely that the large n_{agg} numbers were all formed with segments from different chains. It would mean that chain of molar mass in the range from 1.33×10^5 to 5.5×10^5 g/mol (derived from M_w/n_{agg}) would have established the aggregate, but this would be difficult to reconcile with the observation that aggregation only could be detected for $M_w > 8 \times 10^5$ g/mol. Much more likely the clustered domains partially arose from intramolecular segment packing. The length of these segments could be estimated and was with 75−92 nm, surprisingly constant for the five aggregated samples but fairly large compared to the average radius of gyration and would correspond to about 330 monomer units in an all-trans conformation. This length still is small compared to the overall degree of polymerization, which varies from $DP_w = 2.9 \times 10^3$ to 623.4×10^3. Still chain stiffness is certainly present. The observation with PVIA gives further evidence. This sample has a weight-average molar mass of $M_w = 8 \times 10^5$ g/mol just around the break point of observed insetting aggregation with a 3-fold coil expansion compared to the single chain dimension of nonassociated chains. In fact, with this sample the Kratky plot shows behavior of nearly rigid cylinders.

Two-Particle System in Solution. As was already outlined in the Introduction, the one-component systems of particles with a heterogeneous structure would represent only an extreme limit in the model classification. An alternative consists of the presence of a two-component system in which the two components differ not only in their weight-average molar mass but also significantly in their architecture. The equivalence of the two approaches (one- and two component systems) immediately follows from the basic scattering theory in which the particle scattering function is given by the sum over all pairs of scattering elements

$$P(q) = \frac{1}{N^2}\sum_j^N\sum_k^N\left\langle\frac{\sin(qr_{jk})}{qr_{jk}}\right\rangle \qquad (13)$$

For both, a heterogeneous one-component structure and a mixture of two components, the sum in eq 13 always can be split into two parts. The only difference in the two examples consists of the fact that in a heterogeneous one-component structure some cross-terms are present arising for instance from the globule and the attached chains, whereas these cross-terms no longer are present if the two components in the solution are moving independently of each other. If the globular structure is large compared to the size of linear chains in the particles, the cross-terms are strongly determined by the large component. Because of this it becomes extremely difficult to discriminate between these two possibilities, unless other experimental data or information were available (e.g., when two well-developed peaks were detected in size exclusion chromatography). The observation of two modes of motion in dynamic light scattering is not a proof for two individual components because the fast motion could arise from nonattached chains but also from the internal mode of motion of attached chains. As will be outlined in detail in a separate contribution,[20] we found in dynamic light scattering a weak fast motion which was strongly overshadowed by the strong slow motion of the aggregates.

The problem becomes even more complex if the chains are partially bound to large particles. We still made an attempt of a curve analysis for the case that the large component is governed by a globular structure and the small by coils of linear chains. This approach has its correspondence to the other extreme limit of the on-component consideration and was used by several other colleagues,[11−14] and the reliability was tested by one of the present authors with an example where the experimental individual component parameters could be compared with those from the two-component analysis.[15] The two selections of the Guinier approximation for the global part and the Zimm type for the small component proved to be an excellent choice.[15] Also, the curve analysis with the PVI particles gave very satisfactory fits of the experimental curves and reasonable data—this, however, only with the Zimm-type of angular dependence of the nonattached component.

We considered the limit in which all linear chains are not attached. Despite justified skepticism the curve analysis with a globular structure for the high molar mass and nonattached flexible linear chains gave reasonable data. Compared to other associating systems, where a similar analysis was applied,[11−15] the mass fraction of the aggregates is with about 30% unusually high (see Table 3). Mostly values in the range of a few percent were found. Certainly the large mass fraction of the high-M_{w1} particles is not a small byproduct. The presence of two components was confirmed by dynamic light scattering data where two modes of motion were observed (manuscript in preparation). The two-component curve fit will give a refined answer, for instance, with a soft sphere model with semiflexible spacers, which at present may be the best approximation for the aggregates. The calculations are tedious but appear to be possible.

Linear Mass Density. Really new information was gained when the asymptote of the Casassa−Holtzer plot was examined. With eqs 1 and 2 we find

$$\frac{q}{\pi}M_w P_z(q) \rightarrow m\,\frac{M_{w1}}{L_{w1}} + (1-m)\frac{M_{w2}}{L_{w2}} = \left(\frac{M_w}{L_w}\right)_{exp} \qquad (14)$$

$$n_{agg,1} = [n_{agg}^{exp} - (1-m)]/m \qquad (15)$$

with

$$\left(\frac{M_w}{L_w}\right)_{exp}\Big/\left(\frac{M_{w2}}{L_{w2}}\right) = n_{agg}^{exp}$$

and

$$\left(\frac{M_{w1}}{L_{w1}}\right)\Big/\left(\frac{M_{w2}}{L_{w2}}\right) = n_{agg,1}$$

With the data of Table 3 values for the aggregated component in short junction zones were obtained of $n_{agg,1} = 13$, 109, 56, 49, and 77 (increasing particles mass) or on the average (without the first sample) $\langle n_{agg,1}\rangle = 72$. Although even such large thickness will not yet cause a decrease in the range of light scattering, the value seems to be considerably too large. Very likely the chain behavior that becomes noticeable at large q values is not solely caused by free chains alone, but a marked fraction belongs to the structure of the aggregate, a result that was reasonable to expect. Apparently, the observed aggregate system can be classified in the above-mentioned framework between a one-component heterogeneous structure and a two-component system

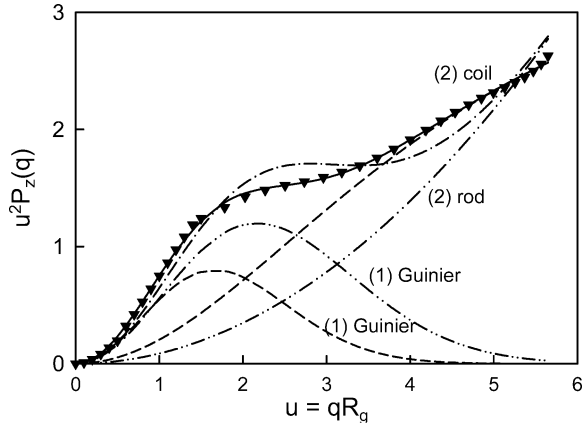

Figure 11. Same type of curve analysis as in Figure 10 for PVIC. This sample exhibited a larger contribution of the compact aggregate component. Again excellent agreement was obtained for coils as the low molar mass component.

in which the heterogeneous aggregates coexists with nonattached linear chains. We think Figure 9 gives a good representation.

What Could be the Reason for the Break in Behavior around a Molar Mass of $M_w \approx 8 \times 10^5$ g/mol? The study of the aggregate structure did not give us many new indications in addition to the information from the measured global polyme properties (R_g, R_h, A_2, and $[\eta]$), but there remain some aspects worth considering. Most likely the occurring stunning break is related to the peculiarities of the precipitating free radical polymerization. The reasons for this were discussed at some length in the preceding paper. Therefore, only some essential points are repeated here. In contrast to common precipitating polymerization, the phase separation of PVI in toluene or benzene corresponds to a *liquid/solid* phase separation. On phase separation in these solvents the PVI molecules immediately pass into a nonswollen glassy state. Therefore, the *dissolution process* has rather to be considered than the increase of molar mass by reduction of the initiator where the chains always are soluble. A dissolution process can strongly be impeded and delayed if special interaction among closely packed chains are effective. A precipitated sample starts to swell in a good solvent, and gradually shorter chains will be eluted first and the solid material partially will transform into large clusters which again gradually become smaller. Once, however, a steric stabilization of the particle is achieved by many dangling chains, a *metastable state* can be obtained in which the particles can stay without further dissolution or association. Such behavior is known for hydrogen-bonded structures as observed with many polysaccharides. We pointed out that observations in the literature caused the authors to deduce hydrogen bonding between the PVI chains.[57] Overberger et al. reported that vinylimidazole and also the polymer tightly binds water that below 100 °C cannot be removed even under stringent drying conditions. Our samples were dried in a vacuum at 10 mmHg and a temperature of 40 °C.[58] Under these circumstances partially hydrated imidazole substituents form hydrogen bonds with its neighbor either in the same chain or with another one in the closely packed precipitant. The former causes a chain stiffening and the latter metastable aggregates. In particular, the dense packing and resulting stiffness of junction zone was realized with these aggregates and this strengthens our hypothesis. Further findings with

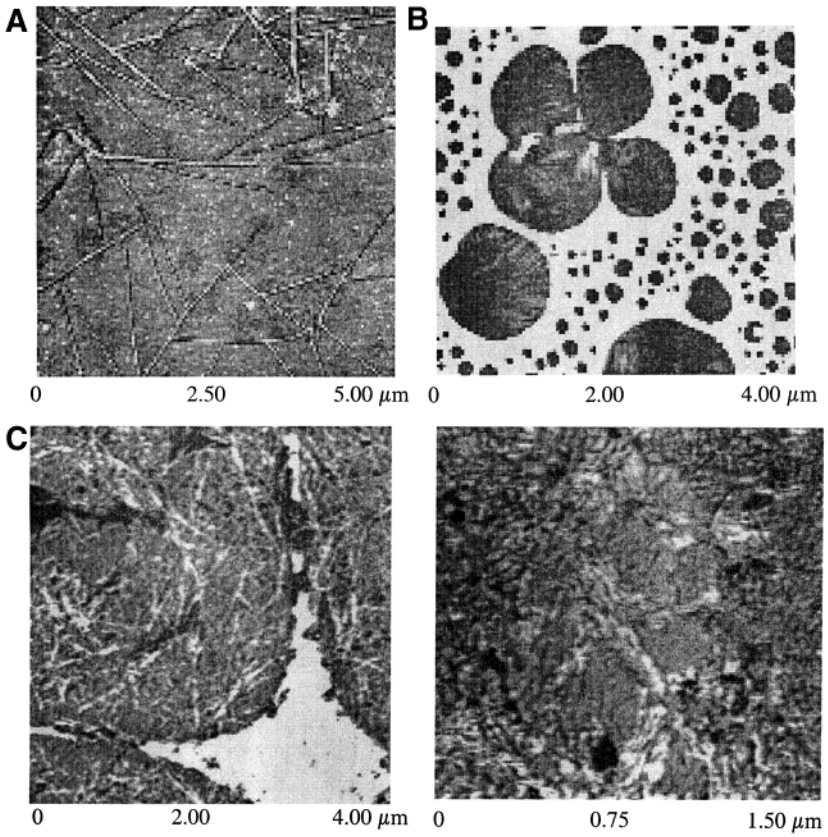

Figure 12. AFM (phase) photographs of three high molar mass PVI aggregates. (A) PVIA; (B) PVIB; (C) PVID: low (left) and high (right) magnification. The samples were prepared by allowing droplets of diluted ethanol solutions (0.1 mg/mL) to dry on freshly cleaved mica surfaces at 40 °C. The measurements were performed with a NanoScope IIIa operating in tapping mode.

not yet published with other polymers and with our observations with PVI in various solvents further support our view. The findings from PVI in *different* solvents will be reported in forthcoming papers.[59]

Conclusion

The evaluation of aggregated structures in solution is a difficult task because no clear a priori predictions can be made. The only way how to proceed consists of a comparison of the experimentally observed angular dependencies with theoretically and experimentally well-studied particle models. We found that the PVI particles are close to the models of stiff star-branched macromolecules and the soft sphere model with Gaussian behavior of the spacer chains. An even better agreement with experiment will become possible when chain stiffness is introduced into the dendric soft sphere model. The obtained similarities allowed us to classify the aggregates as globular heterogeneous structures composed of densely packed stiff chains. Very likely, these aggregates coexist with nonattached linear chains. The deduced chain stiffness is suggested being caused by hydrogen bonding, which results from partially but tightly bound water. Furthermore, it turned out that in the study of large particles in solution associates have to be distinguished from aggregates. Associates are in thermodynamic equilibrium with nonassociated linear chains, whereas aggregates only reach a metastable state.

Addendum. After submitting the paper and during the course of reviewing we had the chance to perform some atomic force microscopy (AFM) from the PVI aggregates in a very dilute ethanol solution ($c = 0.1$ mg/mL). A drop of solutions was put on a mica surface and was dried in an oven at about 40 °C. Parts A, C, and B of Figure 12 show the result from PVIA, PVID, and PVIB. The first two samples displayed in the light scattering typical rodlike behavior, and the last sample was the highest and most compact aggregate, for which we still found in the asymptotic regime of large q typical stiff chain behavior with a remarkable number of chains combined in a bundle. In all three examples these rodlike bundles are clearly seen. Most striking behavior was obtained with PVIA with the extended long cylinders of surprisingly homogeneous thickness. Figure 12A seems to indicate that a network was formed. Certainly such network is not present in the solution which showed typical Newtonian fluid character. Evidently the visible network is an effect of overlap of various clusters during the drying process. Long rods that are vertically attached to another rod via the cross-sectional surface are not stable enough to keep the contact in solution. The smooth thickness of the thin cylinders must be caused by a control mechanism, which still is not known to us. On the whole the structure resembles much those observed with fibrin clusters before the network is formed. Furthermore, all AFM pictures give much evidence for the fact that the large length growth is accompanied by a weak lateral aggregation, which is related to the longer chain length of the macromolecules. A long chain length was to be expected from the decrease in the initiator concentration. The AFM pictures do not fully represent the conditions of a solution, but the findings certainly support our findings by static light scattering. The PVI aggregates represent surprisingly well-defined supramolecular structures, which to our knowledge is the first example for an atactic synthetic linear polymer.

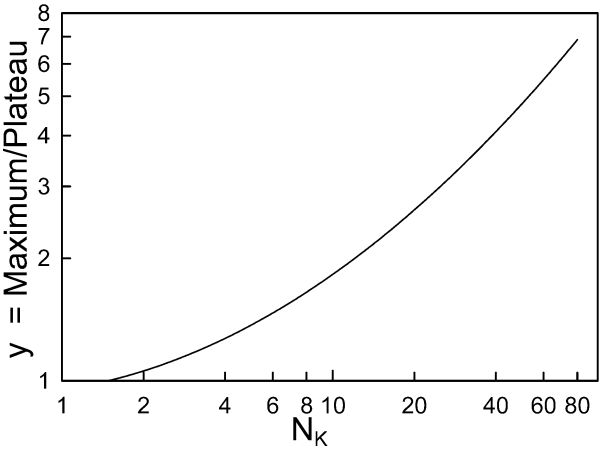

Figure 13. Ratio of the maximum height to that of the asymptotic plateau in the Casassa−Holtzer presentation as a function of the number of Kuhn segments N_K.

Acknowledgment. We are grateful to Dr. Yi Thomannn for her expertise and kind introduction to atomic force microscopy.

Appendix 1

Dependence of the Maximum Height to the Plateau Height on the Number of Kuhn Segments per *Linear Chain*. The Casassa−Holtzer plot $(q/\pi)(R_\theta/Kc) = (q/\pi)M_wP(q)$ as a function of $u = qR_g$ passes for any flexible and semiflexible chains through a maximum as long as the chain is longer than two Kuhn segments and approaches at large q values a plateau. The asymptotic plateau height $M_L = M_w/L_w$ is independent of polydispersity, where L_w is the weight-average contour length. The height of the maximum increases with the number of Kuhn segments per chain. This dependence can be derived from the Koyama theory.[28] Figure 13 shows this dependence for monodisperse linear chains. In the range of 1.5 to about 90 Kuhn segments per chain the curve is represented by the regression curve of the following equation

$$\log y = -0.0218 + 0.09696(\log N_K) + 0.1863(\log N_K)^2 \quad \text{(A1)}$$

For nonlinear chains the asymptotic plateau keeps its value, but the maximum height changes with the macromolecular architecture.

Appendix 2

Soft Sphere Model[32] and Angular Dependence of Scattered Light. The model represents regularly branched strictly monodisperse macromolecules. The first branching generation is the 3-arm star molecule. If each arm branches off with two further branches, the second generation is obtained, etc. The chains connecting two adjacent generation are of the same length and follow Gaussian statistics. Under these conditions the angular dependence is given as follows:

$$S(u) = 1 + 6P_1P_2 + 6[xP_0 + (P_1P_2)^2] + 2F_1 + F_2 - F_3 \quad \text{(A2)}$$

$$P(u) = S(u)/N^2 \quad \text{(A3)}$$

$N = 1 + 3xm$ is the total number of repeating units, $x = (2^n - 1)$ is the number of branching units in the nth

genration, n is the number of generations, and m is the number of repeating units of the linear spacer chains

$$R_g^2 = b^2(3m^3/2N^2)\{x(^1/_3 - 6 + 10n) + 6x^2(n-2) + 4n + [2(x+1)n - 3x]/m\} \quad \text{(A4)}$$

$$P_0 = [my^2 - (1-\Phi^m)]/y^4 \quad \text{(A5a)}$$

$$P_1 = [1 - (y^2)/y^2](1-\Phi^m) \quad \text{(A5b)}$$

$$P_2 = [1 - (2\Phi^m)^n]/(1-2\Phi^m) \quad \text{(A5c)}$$

$$P_3 = \Phi^m[1 - (\Phi^m)^{n-1}]/(1-\Phi^m) \quad \text{(A5d)}$$

$$P_4 = 2\Phi^m[1 - (2\Phi')^{n-1}]/(1-2\Phi^m) \quad \text{(A5e)}$$

$$P_5 = 2\Phi^{2m}/(1-2\Phi^{2m}) \quad \text{(A5f)}$$

$$P_6 = 1/(1-2\Phi^m) \quad \text{(A5g)}$$

$$F_1 = 6P_1^2P_6[(2^{n-1}-1) - 2^{n-1}P_3] \quad \text{(A5h)}$$

$$F_2 = 3P_1^2P_6\Phi^m[(2^n - 2) - P_4]/(1-\Phi^m) \quad \text{(A5i)}$$

$$F_3 = 3P_1^2P_6P_5[2^{n-1}(P_3/\Phi^m) - (2\Phi^m)^{n-1}P_4] \quad \text{(A5j)}$$

where $\Phi = \exp(-y^2)$ with $y^2 = q^2b^2/6$.

Appendix 3

Star-Branched Macromolecules of Semiflexible Arms.[31]

$$P_{star}^{BW}(q) = f^{-1}\{P_N^W(q) + (f-1)[X^{-1}\int_0^X \phi(x,q)\,dx]^2\} \quad \text{(A6)}$$

$$P_N^W(q) = X^{-2}\int_0^X (X-x)\phi(x,q)\,dx \quad \text{(A7)}$$

$$\phi(x,q) = \exp[-(s^2/3)xf(x)]\,\sin(sxg(x))/(sxg(x)) \quad \text{(A8)}$$

where the following reduced variables were used

$$X = 2L/l_K = 2N_K, \quad s = ql_K/2, \quad x = 2t/l_K \quad \text{(A9)}$$

with L the contour length, l_K the Kuhn segment length, and t the contour length from a chain section.

$$xf(x) = 2(\langle r^2\rangle/l_K^2) - xg(x) \quad \text{(A10)}$$

$$xg(x) = 2(\langle r^2\rangle/l_K^2)[10(1 - (3/5)(\langle r^4\rangle/\langle r^2\rangle^2))]^{1/2}/2 \quad \text{(A11)}$$

$$2(\langle r^2\rangle/l_K^2) = x - \exp(-x) \quad \text{(A12)}$$

$$4(\langle r^4\rangle/l_K^4) = (5/3)x^2 - (52/9)x - (2/27)(1-\exp(3x)) + 8(1-\exp(x)) - 2x\exp(-x) \quad \text{(A13)}$$

The transition from Gaussian to rodlike behavior is given by the function $xg(x)$, which in turn is controlled by the ratio of the fourth moment to the square of the second moment of the distance distribution. For large numbers of Kuhn segments N_K the Gaussian chain is obtained; for $N_K \approx 1$ the rigid rod is approached. The model assumes that noncorrelation persists among the various arms such that two arms can be represent by a "broken wormlike" (BW) chain. The individual arms follow the wormlike chain behavior.

References and Notes

(1) Savin, G.; Burchard, W.; Luca, C.; Beldie, C., submitted for publication.
(2) Trappe, V.; Bauer, J.; Weissmüller, M.; Burchard, W. *Macromolecules* **1997**, *30*, 2365.
(3) (a) Flory, P. J. *J. Am. Chem. Soc.* **1941**, *63*, 3083, 3091, 3096. (b) *J. Chem. Phys.* **1942**, *46*, 132. (c) *Principles of Polymer Chemistry*; Cornell University Press: Ithaca, NY, 1953.
(4) (a) Stockmayer, W. H. *J. Chem. Phys.* **1943**, *11*, 65. (b) *J. Chem. Phys.* **1944**, *12*, 125.
(5) Kajiwara, K.; Burchard, W.; Gordon, M. *Br. Polym. J.* **1970**, *2*, 110.
(6) (a) Stauffer, D.; Cognilio, A.; Adams, M. *Adv. Polym. Sci.* **1982**, *44*, 103. (b) Stauffer, D. *Introduction to Percolation Theory*; Taylor & Francis: Philadelphia, PA, 1985.
(7) Kratky, O.; Porod, G. *Recl. Trav. Chim.* **1949**, *68*, 1106.
(8) Guilbot, A.; Mercier, C. Starch. In *The Polaysaccharides*; Aspinall, G. O., Ed.; Academic Press: Orlando, FL, 1985; Vol. 3, Chapter 3.
(9) Schulz, G. V. *Z. Phys. Chem. (Munich)* **1940**, *B46*, 137; *B47*, 155.
(10) Flory, P. J. *Principles of Polymer Chemistry*; Cornell University Press: Ithaca, NY, 1953.
(11) Burchard, W. Light Scattering Techniques. In *Applied Fibre Science*; Happey, F., Ed.; Academic Press: London, 1978; Chapter 10.
(12) Morgenstern B.; Röder, T. *Das Papier* **1998**, *52*, 713.
(13) Helmstedt, M.; Stejskal, J. *Int. J. Polym. Anal. Charact.* **1997** *4*, 219.
(14) Francuskiewicz, F.; Dautzenberg, H. *Eur. Polym. J.* **1985**, *21*, 455.
(15) Aberle, T.; Burchard, W.; Vorwerg, W.; Radosta, S. *Starch/Stärke* **1994**, *48*, 329.
(16) (a) Schulz, L.; Burchard, W.; Dönges, R. Cellulose Deriatives. In Heinze, T. J., Glasser, W. G., Eds.; *ACS Symp. Ser.* **1998**, *688*, 218. (b) Burchard, W. *Adv. Polym. Sci.* **1996**, *64*, 45.
(17) Trappe, V.; Bauer, J.; Weissmüller, M.; Burchard, W. *Macromolecules* **1997**, *30*, 2365.
(18) Galinsky, G.; Burchard, W. *Macromolecules* **1997**, *30*, 6967.
(19) Aberle, L. B.; Kleemeier, M.; Hennemann, O.-D.; Burchard, W. *Macromolecules* **2002**, *35*, 1877.
(20) Savin, G.; Burchard, W., manuscript in preparation (Dynamic LS from PVI in ethanol solution).
(21) Kratky, O.; Porod, G. *J. Colloid Sci.* **1949**, *4*, 35.
(22) Casassa, E. F. *J. Chem. Phys.* **1955**, *23*, 596.
(23) Holtzer, A. *J. Polym. Sci.* **1955**, *17*, 432.
(24) Zimm, B. H. *J. Chem. Phys.* **1948**, *16*. 1999.
(25) Guinier, A. *Ann. Phys.* **1939**, *12*, 161; *Compt. Rend.* **1939**, *208*, 894.
(26) Guinier, A.; Fournet, G. *Small Angle Scattering from X-Rays*; Wiley: New York, 1955.
(27) Goldstein, M. *J. Chem. Phys.* **1953**, *21*, 189.
(28) Schmidt, M.; Paradosi, G.; Burchard, W. *Makromol. Chem., Rapid Commun.* **1985**, *6*, 767.
(29) Koyama, R. *J. Phys. Soc. Jpn.* **1973**, *34*, 1029.
(30) Denkinger, P.; Burchard, W. *J. Polym. Sci., Phys. Ed.* **1991**, *29*, 589.
(31) Huber, K.; Burchard, W. *Macromolecules* **1989**, *22*, 3332.
(32) Burchard, W.; Kajiwara, K.; Nerger, D. *J. Polym. Sci., Phys. Ed.* **1982**, *20*, 157.
(33) Daoud, M.; Martin. J. E. In *The Fractal Approach to Heterogeneous Chemistry*; Aveni, D., Ed.; Wiley: New York, 1889.
(34) Richter, D.; Stühn, B.; Ewen, B.; Nerger, D. *Phys. Rev. Lett.* **1987**, *58*, 2462.
(35) Glatter, O.; Kratky, O. *Small Angle X-Ray Scattering*; Academic Press: London, 1982.
(36) Higgins, J. S.; Benoit, H. *Polymers and Neutron Scattering*; Clarendon Press: Oxford, 1994.
(37) Herzog, B.; Huber, K.; Stegemeier, H. *Langmuir* **2003**, *19*, 5223.
(38) De Gennes, P.-G. Scaling *Concepts in Polymer Physics*; Cornell University Press: Ithaca, NY, 1979.
(39) Lang, P.; Burchard, W.; Wolfe, M. S.; Spinelli, H. J.; Page, L. *Macromolecules* **1991**, *24*, 1306.
(40) Molina, L. A. Rey, A.; Freire, J. J. *Comput. Theor. Polym. Sci.* **1998**, *17*, 243.
(41) Allegra, G.; Ganazzoli, F. *Adv. Chem. Phys.* **1989**, *75*, 265.

(42) Allegra, G.; Ganazzoli, F. *Macromolecules* **1993**, *26*, 330.
(43) Ganazzoli, F.; Allegra, G.; Colombo, E.; DeVitis, M. *Macromolecules* **1995**, *28*, 1076.
(44) Ganazzoli, F. *Macromol. Symp.* **2002**, *190*, 53.
(45) Huber, K.; Burchard, W.; Bantle, S.; Feters, L. J. *Polymer* **1987**, *28*, 1997.
(46) Flory, P. J. *Statistical Mechanics of Chain Molecules*; Interscience: New York, 1969.
(47) (a) Nerger, D. Ph.D. Thesis University of Freiburg, Germany, 1978. (b) Schmidt, M.; Nerger, D.; Burchard, W. *Polymer* **1979**, *20*, 582. (c) Burchard, W. *Adv. Polym. Sci.* **1983**, *48*, 85.
(48) Horkay, F.; Burchard, W.; Geissler, E.; Hecht, A.-M. *Macromolecules* **1993**, *26*, 1296.
(49) Coviello, R.; Burchard, W.; Geissler, E.; Maier, D. *Macromolecules* **1997**, *30*, 2008.
(50) Zimm, B. H.; Stockmayer, W. H. J. *Chem. Phys.* **1949**, *17*, 1301.
(51) Reference 47c, pp 88−91.
(52) (a) Rees, D. A. *Adv. Carbohydr. Chem.* **1969**, *24*, 267. (b) *Chem. Ind.* **1972**, 630. (c) *Carbohydr. Polym.* **1982**, *2*, 254.
(53) Smidsröd, O. Grandalen, H. *Carbohydr. Polym.* **1982**, *2*. 270.
(54) (a) Coviello, T.; Kajiwara, K.; Burchard, W.; Dentini, M.; Crescenzi, V. *Macromolecules* **1986**, *19*, 2826. (b) Coviello, T.; Burchard, W.; Dentini, M.; Crescenzi, V. *Macromolecules* **1987**, *20*, 1102.
(55) Dentini, M.; Coviello, T.; Burchard, W. Crescenzi, V. *Macromolecules* **1988**, *21*, 3312.
(56) Coviello, T.; Burchard, W.; Dentini, M.; Crescenzi, V.; Morris, V. J. *J. Polym. Sci., Polym. Phys* **1995**, *33*, 1833.
(57) Lippert, J. L.; Robertson, J. A.; Havens, J. R.; Tan, J, S. *Macromolecules* **1985**, *18*, 63.
(58) (a) Overberger, C. G.; Vorchheimer, N. *J. Am. Chem. Soc.* **1963**, *85*, 951. (b) Overberger, C. G.; Vorchheimer, N.; Yaralavsky, S. *J. Am. Chem. Soc.* **1965**, *87*, 296.
(59) Savin, G.; Burchard, W. Manuscript in preparation (PVI in various solvents).

MA0353639